Dislocation Dynamics in Aluminium and in Aluminium-Copper Alloys

Tamler, H.; Kanert, O.; Alsem, W.H.M.; De Hosson, J.T.M.

Published in:
Acta Metallurgica

DOI:
10.1016/0001-6160(82)90173-0

Publication date:
1982

Acta metall. Vol. 30, pp. 1523 to 1536, 1982
Printed in Great Britain.

0001-6160 82 081523-14$03.00/0

DISLOCATION DYNAMICS IN ALUMINIUM AND IN ALUMINIUM–COPPER ALLOYS: A NUCLEAR MAGNETIC RESONANCE AND TRANSMISSION ELECTRON MICROSCOPIC STUDY

H. TAMLER and O. KANERT

Institute of Physics, University of Dortmund, 46 Dortmund—50, FRG

and

W. H. M. ALSEM and J. Th. M. DE HOSSON

Department of Applied Physics, Materials Science Centre, University of Groningen, Nijenborgh 18, 9747 AG Groningen, The Netherlands

(*Received* 19 *October* 1981; *in revised form* 11 *February* 1982)

Abstract—Pulsed nuclear magnetic resonance techniques as well as transmission electron microscopy have been applied to study dislocation motion in ultrapure aluminium and aluminium–copper alloys (Al:xCu with x_{max} = 1 at.%). The spin-lattice relaxation rate in the rotating frame, $T_{1\rho}^{-1}$ of ^{27}Al has been measured as a function of the plastic strain rate $\dot{\epsilon}$ at 77 K. For finite strain rates $\dot{\epsilon}$, the movement of dislocations induces an additional relaxation rate arising from time fluctuations in the nuclear quadrupole interaction. From this motion-induced part of the relaxation rate the mean free path L of mobile dislocations can be calculated which is determined by the distribution of lattice defects acting as obstacles for moving dislocations. The NMR experiments are combined with transmission electron microscopic investigations to reveal the static structure of defects in the samples. Correlations between the *in situ* observed mean free path L of mobile dislocations and between the microscopic defect structure arising from the ageing process (θ' phase, solid solution) and the degree of plastic deformation ϵ are shown. It turns out that in the θ' phase at small strains L is determined by the microstructure and is equal to the mean separation between the precipitates. For large strains L is determined by the statistical distribution of the dislocation loops lying between the precipitates. On the other hand, in ultrapure aluminium L is determined by the dislocation cell structure.

Résumé—Nous avons étudié le mouvement des dislocations dans l'aluminium ultrapur et des alliages d'aluminium et de cuivre (Al:xCu avec x_{max} = 1 at.%), par résonance magnétique nucléaire pulsée et microscopie électronique par transmission. Nous avons également mesuré la vitesse de relaxation spin-réseau dans le repère tournant, $T_{1\rho}^{-1}$ d' ^{27}Al en fonction de la vitesse de déformation plastique $\dot{\epsilon}$ à 77 K. Pour des vitesses de déformation finies $\dot{\epsilon}$, le mouvement des dislocations induit une vitesse de relaxation additionnelle provenant des fluctuations de l'interaction nucléaire quadripolaire en fonction du temps. Pour cette partie de la vitesse de relaxation induite par le déplacement des dislocations, on peut calculer le libre parcours moyen L des dislocations mobiles, qui est déterminé par la répartition des défauts réticulaires agissant comme obstacles d'opposant au déplacement des dislocations. La RMN, associée à la microscopie électronique par transmission, permet de révéler la structure statique des défauts dans les échantillons. Nous présentons les corrélations qui existent entre le libre parcours moyen L des dislocations libres observé *in situ*, la structure microscopique des défauts provenant du vieillissement (phase θ', solution solide) et le degré de déformation plastique ϵ. Dans la phase θ' et pour de faibles déformations, nous déterminons L à partir de la microstructure: il est égal à la séparation moyenne entre les précipités. Dans le cas des fortes déformations, L est déterminé par la répartition statistique des boucles de dislocations situées entre les précipités. Par contre, dans l'aluminium ultrapur, L est déterminé par la structure des cellules de dislocations.

Zusammenfassung—Die Versetzungsbewegung in ultrareinem Aluminium und in Aluminium–Kupfer-Legierungen (Al:xCu mit x_{max} = 1 At.%) wurde mit Pulstechniken der Kernspinresonanz und mittels Durchstrahlungselektronenmikroskopie untersucht. Die Spin-Gitter-Relaxationsrate $T_{1\rho}^{-1}$ im rotierenden System von ^{27}Al wurde in Abhängigkeit von der Abgleitungsgeschwindigkeit $\dot{\epsilon}$ bei 77 K gemessen. Bei endlichen Abgleitgeschwindigkeiten erzeugt die Bewegung der Versetzungen eine zusätzliche Relaxationsrate, die von Zeitfluktuationen in der Kernquadrupol-Wechselwirkung herrühren. Aus diesem bewegungsinduzierten Anteil der Relaxationsrate läßt sich der mittlere, von den als Hindernisse wirkenden Gitterfehlern bestimmte Laufweg L der beweglichen Versetzungen errechnen. Diese Experimente werden mit elektronenmikroskopischen Beobachtungen der Defektstruktur der Proben ergänzt. Es werden Zusammenhänge aufgezeigt zwischen dem *in-situ* beobachteten Laufweg und der mikroskopischen Defecktstruktur, die von einem Auslagerungsprozess (θ'-Phase, Mischkristall) und der plastischen Abgleitung ϵ herrührt. Im Falle der θ'-Phase ist der mittlere Laufweg L bei kleinen Abgleitungen bestimmt durch die Mikrostruktur und gleich dem mittleren Abstand zwischen den Ausscheidungen. Bei großer Abgleitung ist L gegeben durch die statistische Verteilung der Versetzungsschleifen zwischen den Ausscheidungen. In ultrareinem Aluminium ist L dagegen durch die Versetzungszellstruktur bestimmt.

1. INTRODUCTION

Characteristics in the mechanical behaviour of crystals are controlled by the collective behaviour of dislocations. Therefore, knowledge of dislocation dynamics can be used to predict macroscopic mechanical properties of materials. Especially, plastic deformation of crystals is due to the (thermally activated) motion of a large number of mobile dislocations with density ρ_m moving in the field of external and internal stresses where the latter are caused by obstacles such as forest dislocations and impurities.

At first, Orowan [1] interpreted the mechanism of plastic flow as a dynamical process. The theory smears all dislocations in a crystal into a homogeneous distribution described by a (strain-dependent) density function ρ_m and an (stress-dependent) average velocity $\bar{v}$. Then, the plastic strain rate $\dot{\epsilon}$ can be written as

$$\dot{\epsilon} = \phi \cdot b \cdot \rho_m \cdot \bar{v} \tag{1}$$

where b is the magnitude of the Burgers vector and ϕ is a geometrical factor relating the shear strain a to the strain ϵ.

The microscopic characteristics of dislocation motion are governed by the strength and the distribution of obstacles, the actual stress and temperature. Assuming the actual jump time τ_j to be small compared to the mean time of stay τ_w at an obstacle the motion may be considered to be jerky-like. Then, equation (1) may be written as

$$\dot{\epsilon} = \phi \cdot b \cdot \rho_m \cdot L/\tau_w \tag{2}$$

where L denotes the mean jump distance between obstacles which are considered to be uniform. A wide variety of experimental techniques have been used in the past for studying the *microscopic* behaviour of dislocation motion. In 1959, Johnston and Gilman [2] have applied the etch pit method for measuring the mean velocity $\bar{v}$ of a single dislocation as a function of applied stress and temperature. Neuhäuser *et al.* [3] have introduced the high-speed cinematography for the determination of velocity and local density of mobile dislocation within slip bands in copper and copper alloys. Observation of acoustic emission associated with dislocation dynamics can be used to analyze the microscopic behaviour of dislocation motion [4]. For instance, by means of this technique Imanaka *et al.* [5] have reported that macroscopic deformation in f.c.c. metals proceeds by a collective motion of groups of dislocations. Internal friction experiments as introduced by Granato and Lücke [6] are able to give information about the strength, density and distribution of pinning obstacles for mobile dislocations. At least, a large number of electron microscopic investigations deals with the observation of static slip line structures and dislocation density including the distribution of dislocations [7] but also with the dynamical behaviour of dislocations under the influence of external stresses [8].

In the past we have shown that nuclear magnetic resonance (NMR) is a useful tool for *in situ* investigations of dislocation motion in non-metallic [9, 10] as well as in metallic [11, 12] materials. In the work, the nuclear spin relaxation rate in the rotating frame, $T_{1\rho}^{-1}$, has been instantaneously measured while a sample is plastically deforming with a constant deformation rate $\dot{\epsilon}$.

In particular, results have been presented as a function of strain rate, of the direction of deformation with respect to the crystal axes, and of temperature. Parallel to the experimental work, the theoretical basis for evaluation of the experimental data has been established [12]. It turned out that from such NMR experiments two informations of the microscopic mechanism of dislocation motion can be obtained in principle: (i) the mean jump distance L and (ii) the mean time of stay τ_w between two consecutive jumps of a mobile dislocation.

In this paper, a comprehensive study of the mechanism of motion of dislocations, resisted by different kinds of barriers in aluminium and aluminium based copper alloys is presented.

For that purpose, *static* transmission electron microscopic observations of the instantaneous dislocation configuration and of the distribution and arrangement of copper in the aluminium matrix are related to *in situ* nuclear spin relaxation measurements. Combining the evaluation of the two sets of data leads to detailed information of the effective mean jump distance L of mobile dislocations.

2. THEORETICAL BACKGROUND

While deforming a sample with a constant strain rate $\dot{\epsilon}$ the spin-lattice relaxation rate in a weak rotating field H_1 ('locking field'), $1/T_{1\rho}$, of the resonant nuclei in the sample is enhanced due to the motion of dislocations. The resulting total relaxation rate may be decomposed into a background relaxation rate, $(1/T_{1\rho})_0$ and the contribution $(1/T_{1\rho})_D$ which is governed by the mechanism of dislocation motion, i.e. by equation (2)

$$\frac{1}{T_{1\rho}} = \left(\frac{1}{T_{1\rho}}\right)_0 + \left(\frac{1}{T_{1\rho}}\right)_D. \tag{3}$$

In metals and alloys, $(1/T_{1\rho})_0$ is due to fluctuations in the conduction electron-nucleus interaction leading to the Korringa relation $(T_{1\rho})_0 \cdot T = c$, where the magnitude of the constant c depends slightly on the strength of the locking field H_1 [13]. In Table 1 the actual values of c are given for the samples under investigation, measured at $T = 77$ K (see section 3).

At a finite plastic strain rate, dislocations move in the crystal, i.e. causing time fluctuations both of the quadrupolar and dipolar spin Hamiltonian for spins with $I > \frac{1}{2}$. However, the dipolar effects on the resulting nuclear spin relaxation due to dislocation motion are negligible and quadrupolar interactions dominate the relaxation behaviour [12]. Furthermore, in the

range of deformation rates applied here the atomic movements involved in dislocation motion are in the so-called ultra-slow motion region, where the Zeeman spin-lattice relaxation rate T_1^{-1} and the spin-spin relaxation rate T_2^{-1} are not remarkably influenced by dislocation motion and where the rotating-frame relaxation rate $T_{1\rho}^{-1}$ is the most appropriate NMR parameter affected by such motions. The resulting expression for the relaxation rate $(1/T_{1\rho})_D$ induced by dislocation motion is given by [11]

$$\left(\frac{1}{T_{1\rho}}\right)_D = \frac{\delta_Q}{H_1^2 + H_{L\rho}^2} \cdot \langle V^2 \rangle \cdot g_Q(L) \cdot \frac{\rho_m}{\tau_w}. \tag{4}$$

Here

$$\delta_Q = \frac{3}{320} \cdot \left(\frac{eQ}{\gamma\hbar}\right)^2 \cdot \frac{2I+3}{I^2(2I-1)} \tag{4a}$$

is a quadrupole coupling constant (Q: nuclear quadrupole moment, I: nuclear spin, γ: gyromagnetic ratio) and $\langle V^2 \rangle$ denotes the second moment of the electric field gradient due to the stress field of a dislocation of unit length [13].

In continuum approximation, $\langle V^2 \rangle$ may be expressed as [14]

$$\langle V^2 \rangle = \int_{r_c}^{R_0} \int_0^{2\pi} r \, dr \, d\theta \, V^2(r, \theta), \tag{4b}$$

where $V(r, \theta)$ is the electric field gradient at a nuclear site with coordinates (r, θ) with respect to a given dislocation, the inner cut-off radius r_c is given by $r_c \simeq 3b$, and the outer cut-off radius R_0 is determined by the total density of the dislocations, $\rho_T: R_0 = (\pi \cdot \rho_T)^{-\frac{1}{2}}$. $H_{L\rho}$ is the mean local field in the rotating frame determined by the local dipolar field $H_{D\rho}$ and the local quadrupolar field $H_{Q\rho}$

$$H_{L\rho}^2 = H_{D\rho}^2 + H_{Q\rho}^2. \tag{4c}$$

The quadrupolar geometry factor $g_Q(L)$ in equation (4) which depends on the mean step width L was calculated by Hut for NaCl [9, 12]. The result of the computer-calculation is presented in Fig. 1 where the jump distance L is expressed in units of the Burgers vector b: $N = L/b$. Typically, in plastic deformation experiments the jump distance L is of the order of $10^{-5} \div 10^{-4}$ cm, i.e. N is of the order of 10^3. For such large jump distances $g_Q(L)$ approaches to one being not very sensitive to a change in L. Furthermore, in the following we will assume that $g_Q(L)$ is not a sensitive material-dependent quantity. The values for $g_Q(L)$ originally calculated for NaCl will be used in the case of Al.

It has to be noted, that equation (4) is valid only in the 'strong-collision region' where the dislocation motion is slow enough to allow the spins to establish a common spin temperature between successive dislocation jumps. In practice, the condition is fulfilled for strain rates $\dot{\epsilon}$ up to about $10\,s^{-1}$ depending slightly on $H_1^2 + H_{L\rho}^2$ [12].

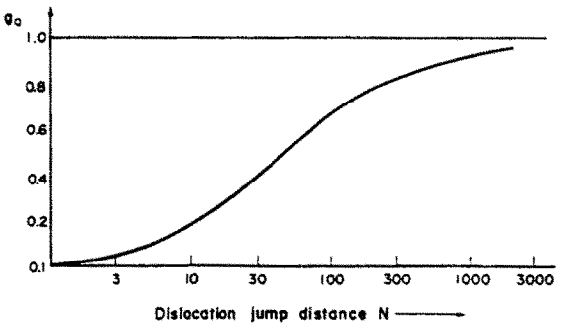

Fig. 1. Quadrupolar geometry factor g_Q for a mobile dislocation as a function of the normalized jump distance N (in units of the Burgers vector).

For ^{27}Al in aluminium, the quadrupole coupling constant δ_Q [equation (4a)] has the value ($Q = 0.15$ barn; $\gamma = 7.035 \cdot 10^3\ G^{-1}\,s^{-1}$) $2.85 \cdot 10^{-25}\ G^2\,\text{dyne}^{-1}\,\text{cm}^4$. The value of $\langle V^2 \rangle$ may either be determined theoretically by means of the corresponding theoretical expression of $V(r, \theta)$ for dislocations as given by Kanert and Mehring [15] or derived experimentally from analysis of the line shape of the NMR signal of the sample which is quadrupole distorted by a known number of dislocations. In the first case, starting from $V(r, \theta) = \mu b/2\pi \cdot C_{11} \langle f^2(\theta) \rangle^{\frac{1}{2}} \cdot r^{-1}$ (μ: shear modulus, C_{11}: gradient-elastic constant, $f(\theta)$: orientation function) equation (4b) may be rewitten as

$$\langle V^2 \rangle = \frac{1}{2\pi} (\mu \cdot b \cdot C_{11})^2 \cdot \langle f^2 \rangle \cdot \ln \frac{R_0}{r_c}. \tag{5}$$

Then, for ^{27}Al in aluminium the mean-squared EFG $\langle V^2 \rangle$ of a dislocation of unit length is given by ($b = 2.86 \cdot 10^{-8}$ cm, $\rho_T = 10^{10}\,\text{cm}^{-2}$, $C_{11} = 7 \cdot 10^3\,\text{dyne}^{-\frac{1}{2}}$, $\mu = 2.8 \cdot 10^{11}\,\text{dyne cm}^{-2}$) $\langle V^2 \rangle = 1.05 \cdot 10^{15}\,\text{dyne cm}^{-2}$ or, introducing the quadrupole factor $A_Q = \delta_Q \cdot \langle V^2 \rangle$: $A_Q|_{\text{Theory}} = 3.0 \cdot 10^{-10}\ G^2\,\text{cm}^2$. On the other hand, A_Q is shown to be given by the relation [12, 15]

$$A_Q = \frac{\langle H_Q^2 \rangle}{\rho_T} \tag{6}$$

where $\langle H_Q^2 \rangle$ denotes the mean-squared local quadrupole field due to dislocations of total density ρ_T. From experimental NMR and X-ray data in plastically deformed aluminium, as published by Kanert and Preusser [16] both $\langle H_Q^2 \rangle$ and ρ_T can be estimated roughly: $\langle H_Q^2 \rangle = 8.25\ G^2$; $\rho_T \simeq 2.8 \cdot 10^{10}\,\text{cm}^{-2}$. Therefore, $A_Q|_{\text{Exp.}} = 2.95 \cdot 10^{-10}\,G^2\,\text{cm}^2$. Comparison of the two values for A_Q determined independently shows a fair agreement.

Finally, combining Orowan's relation (2) with equation (4) one obtains

$$\left(\frac{1}{T_{1\rho}}\right)_D = \frac{A_Q}{H_1^2 + H_{L\rho}^2} \cdot \frac{1}{\phi \cdot b} \cdot \frac{g_Q(L)}{L} \dot{\epsilon}. \tag{7}$$

Hence, for a given plastic-strain rate $\dot{\epsilon}$ the dislocation induced spin relaxation rate is proportional to the

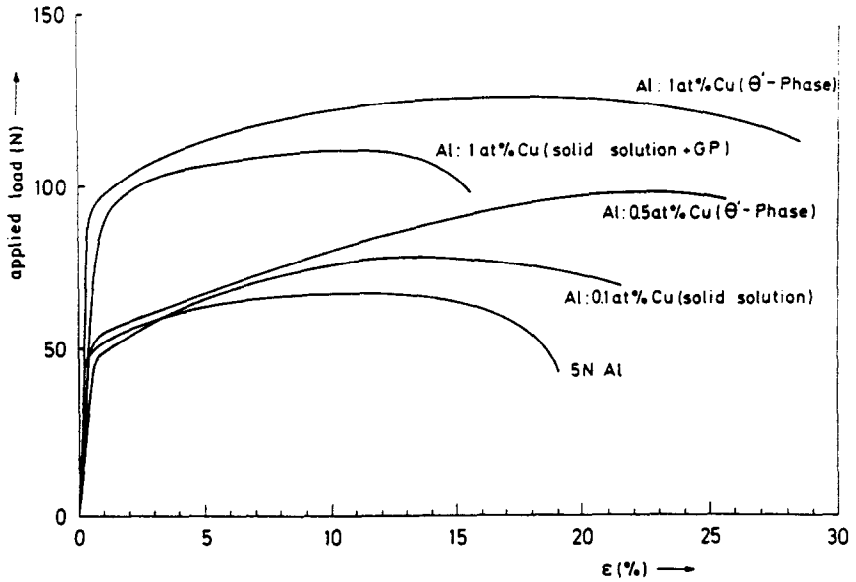

Fig. 2. Deformation curves of *some* of the samples measured at 77 K. (Cross section at the beginning of deformation is 0.6 mm^2 and $\dot{\epsilon} = 10^{-2}\,s^{-1}$.)

inverse of the mean jump distance L. This relationship is used in the experiments discussed below to determine L.

3. EXPERIMENTAL DETAILS

3.1 *Sample-preparation and transmission electron microscopic measurements*

For the investigation, polycrystalline samples with a grain size of the order of 100–200 μm were used. To avoid skin effect distortions of the NMR signal each sample consisted of a single rectangular foil with a length of 27 mm, a width of 12 mm, and a thickness of about 50 μm. The starting material for the samples was (a) 5 N aluminium, (b) 5 N Al: 0.1 at.% Cu, (c) 5 N Al: 0.5 at.% Cu, and (d) 5 N Al: 1 at.% Cu. After a homogenizing procedure at 550°C for 2.5 days the material was rolled out to thin foils with a thickness of about 50 μ and has than been cut by spark erosion to the sample size given above.

Then, the samples (a) consisting of ultrapure aluminium were annealed a second time at 290°C for 1 h. The aluminium–copper alloys were treated in two different ways. In order to get samples of solid solution with a concentration of copper corresponding to materials (b)–(d) the foils were annealed at 550°C for 2.5 h and then quenched to 20°C. A part of these samples was exposed to a third heat treatment in order to produce plate-like precipitates of copper in the samples (θ'-phase in the Al:Cu phase diagram [17, 18]): 5 N Al:0.5 at.% Cu samples were aged at 170°C for 7 days, respectively, whereas 5 N Al:1 at.% Cu samples were heat treated at 200°C for 1 day.

Figure 2 exhibits deformation curves of *some* of the samples measured at 77 K. In particular, the data demonstrate the different plastic behaviour of the Al:1 at.% Cu (solid solution) sample and of Al:1 at.% Cu (θ'-phase). In contrast to the solid solution sample, the sample with precipitates of copper can be plastically deformed up to about 28%.

Transmission electron micrographs were taken by using either a JEM 200CX operating at 160 keV or a Philips EM 300 operating at 100 keV.

3.2 *NMR measurements*

Although the principle of the experiment looks simple, the technical feasibility is not. Figure 3 exhibits the block diagram of the combined tensile machine and NMR spectrometer. In the NMR experiment, the sample under investigation is plastically deformed by a servo-hydraulic tensile machine (ZONIC Technical Lab. Inc., Cincinnati) of which the exciter head XCI TE 1105 moves a driving rod with a constant velocity. The movement is controlled by a digital function generator which serves the Master controller of the exciter head. The data of the mechanical system are as follows: maximum load 5000 N; minimum piston speed: 10 μm s^{-1}; maximum piston speed: 3.10^5 μm s^{-1}; stroke of the piston digital controlled between 1 and 8000 μm, resolution (depending slightly on the gain of the electrohydraulic feedback system): 2–4 μm.

While the specimen was deforming, ^{27}Al nuclear spin relaxation measurements were carried out by means of a BRUKER pulse spectrometer SXP 4-100 operating at 15.7 MHz corresponding to a magnetic field of 1.4 T controlled by a NMR stabilizer (BRUKER B-SN 15).

The NMR head of the spectrometer consisting of a flat rf coil of silver and of tuning elements and the frame in which the rod moves formed together a unit

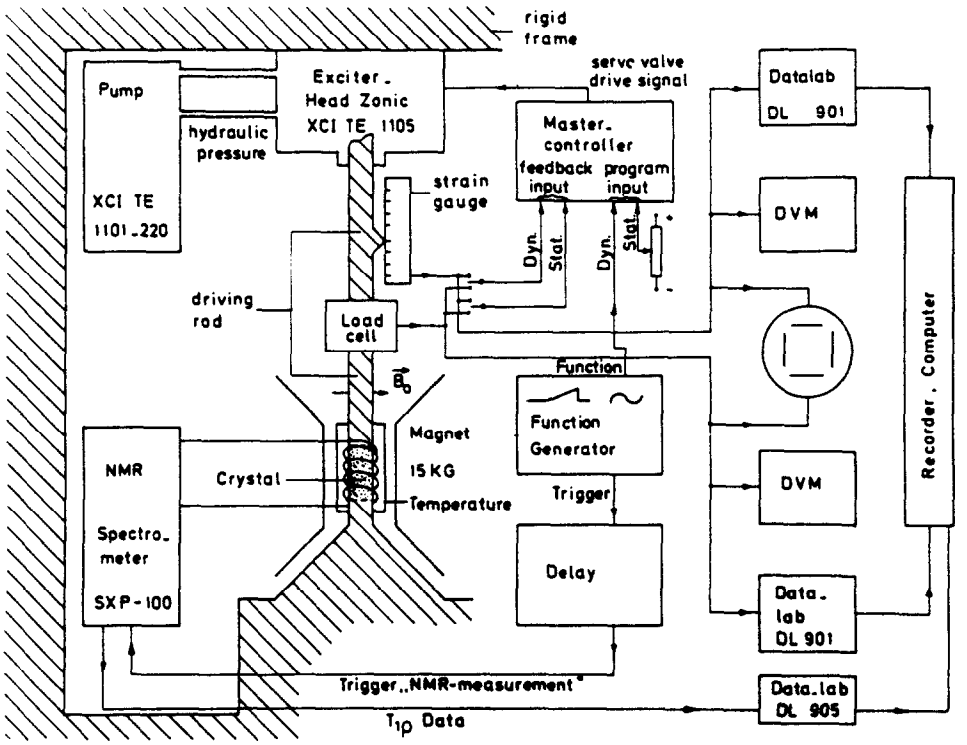

Fig. 3. Scheme of the experimental set-up.

which was inserted between the pole pieces of the electromagnet of the spectrometer. The unit could be temperature-controlled between 77 K and room temperature using a flow gas system. As shown in the block diagram, the spectrometer was triggered by the electronic control of the tensile machine. The trigger starts the nuclear spin relaxation experiment at a definite time during the deformation determined by the delay time of the trigger pulse. Immediately before and after the plastic deformation the magnitude of the background (conduction-electron) relaxation time $(T_{1\rho})_0$ was measured. By means of equation (3), from the experimental $T_{1\rho}$-data the dislocation-induced contribution of the relaxation time, $(T_{1\rho})_D$, could be determined.

During the deformation experiment, the acting load and the resulting plastic deformation are measured separately and simultaneously. As shown by the block diagram in Fig. 3, the different NMR signals as well as the mechanical data were stored in fast transient recorders (DATALAB DL 901/905) and then transcribed on magnetic tape. Further processing of the data was carried out by an on-line VARIAN 620 L-computer.

The following test measurement, important for such type of NMR experiments on metallic samples, was made: to be sure that the increase in the nuclear spin relaxation rate $1/T_{1\rho}$ during the plastic deformation with $\dot{\epsilon} =$ constant is caused actually by internal atomic motions and not by any kind of external electrodynamic effects, the relaxation rate was measured while moving the whole sample with a constant velocity but without any deformation. No change within experimental error in the relaxation rate was observed in such an experiment.

Generally, the NMR measurements discussed here were carried out at $T = 77$ K. At such a low temperature nuclear spin relaxation effects due to diffusive atomic motions are negligible. To show this in more detail one has to start from the Einstein–Smoluchowsky relation connecting the diffusion coefficient D with the mean time of stay τ of an atom between two diffusion jumps (neglecting correlation effects)

$$D = \frac{a^2}{6\tau} \tag{8}$$

(a: jump distance of the atom for the particular diffusion mechanism; for an estimation as done here a may be assumed to be equal to the lattice constant). The self-diffusion coefficient D_{SD} as well as the impurity diffusion of Cu in aluminium, D_{CU}, are published in the literature [21, 22]. From these data and using equation (8) the correlation times τ for diffusive atomic jumps of an aluminium atom and a copper atom, respectively, in the aluminium matrix can be calculated at $T = 77$ K. The correlation times calculated for Al and Cu show that Al and Cu atoms are actually immobile at 77 K, ($\tau > 10^{70}$ s).

These times are much larger than typical values of τ_w for mobile dislocations, which are about 10^{-4} s for $\dot{\epsilon} \approx 1\,\mathrm{s}^{-1}$. Therefore, an observable contribution of diffusive atomic motions to the measured relaxation rates does not occur.

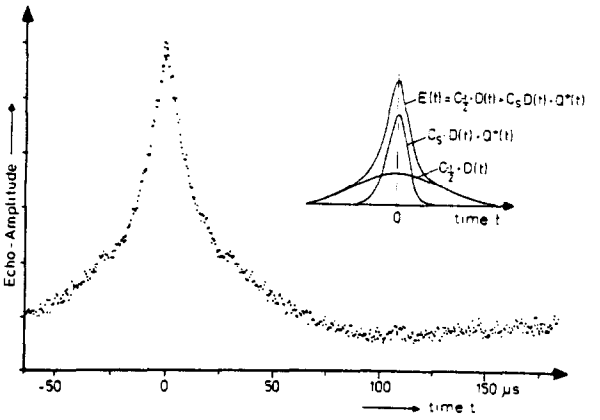

Fig. 4. ^{27}Al spin echo in Al: 1 at.% Cu at 77 K. For $I = 5/2$ $C_{-\frac{1}{2}} = 0.247$ and $C_5Q^*(t) = 0.469\,Q(2t) + 0.284\,Q(4t)$, see equation 9a.

In order to obtain the static local fields $H_{D\rho}$ and $H_{Q\rho}$, respectively, of the samples [see equations (4 and 4c)] the ^{27}Al spin echo signal of the samples was measured. As shown by Kanert and Mehring [15] for $I = 5\,2$ (the nuclear spin quantum number of ^{27}Al) a $\pi/2$-τ-40° pulse sequence induces a spin echo signal at $t = 2\tau$ which may be expressed in a normalized representation as

$$E(t) = 0.247 \cdot D(t) + (0.469 \cdot Q(2t) + 0.284 \cdot Q(4t)) \cdot D(t) \tag{9a}$$

with $E(0) = 1$. Here $D(t)$ denotes the Fourier cosine transformation of the dipolar broadening function $g_D(\omega)$ and $Q(t)$ is the corresponding transform of the quadrupole broadening function $g_Q(a)$.

$$D(t) = \int_{-\infty}^{+\infty} g_D(\omega)\cos(\omega t)\,\mathrm{d}\omega; \quad D(0) = 1 \tag{9b}$$

$$Q(nt) = \int_{-\infty}^{+\infty} g_Q(a)\cos(n \cdot at)\,\mathrm{d}a; \quad Q(0) = 1; \quad n = 2, 4 \text{ [see equation (9a)]} \tag{9c}$$

where the quadrupole distortion frequency a is given by

$$a = \frac{3eQ}{4I(2I-1)\hbar} \cdot V_{zz} \tag{10}$$

(V_{zz}: component of the electric field gradient tensor due to lattice distortions in the direction of the external magnetic field). The dipolar function $D(t)$ as well as the quadrupolar function $Q(t)$ can be expressed to a fair approximation by Gaussian functions [15]

$$D(t) = \exp\left(-\frac{\Delta_D^2}{2}t^2\right) \tag{11a}$$

$$Q(t) = \exp\left(-\frac{\Delta_Q^2}{2}\cdot t^2\right) \tag{11b}$$

where Δ_D^2 and Δ_Q^2 are the second moments of the dipolar broadening function $g_D(\omega)$ and of the quadrupolar broadening function $g_Q(a)$, respectively. From the second moments, the local fields in the rotating frame can be obtained by using the general relation [19]

$$H_{L\rho}^2 = \tfrac{1}{3}\Delta^2. \tag{12}$$

An example of a spin echo signal is given in Fig. 4. The figure shows the spin echo signal of ^{27}Al in an Al: 1 at.% Cu alloy. The second moments Δ_D^2 and Δ_Q^2 were determined by fitting the measured echoes of the different samples by means of equation (9a). The analysis leads to a value for the dipolar second moment Δ_D of about 3.3 G in good agreement with the value determined by Rowland and Fradin [20]. It should be noted that the experimental value of Δ_D in polycrystalline aluminium is remarkably larger than the value obtained theoretically by means of Van Vleck's formula [19], which gives 2.9 G. Up to now, the discrepancy observed first by Rowland and Fradin is unsolved.

Contrary to the dipolar second moment Δ_D^2, the quadrupolar second moment Δ_Q^2 depends on the lattice distortion in the sample due to dislocations and impurity atoms like copper. Therefore, the total local field in the rotating frame, $H_{L\rho}$, increases slightly with increasing concentration of copper in the samples. This is shown in Table 1 where $H_{L\rho}$ was determined

Table 1. Values of Korringa constants c and of local fields in the rotating frame, $H_{L\rho}$, of ^{27}Al in aluminium samples under investigation, measured at 77 K (see section 3)

System	$c \cdot [Ks]$	$H_{L\rho}(G)$
5 N aluminium	1.85 ± 0.1	3.16 ± 0.6
Al:0.1 at.% Cu	1.85 ± 0.1	3.3 ± 0.6
Al:0.5 at.% Cu	1.95 ± 0.1	3.9 ± 0.8
Al:1 at.% Cu	2.05 ± 0.1	4.4 ± 0.9

from the experimental data Δ_D, and Δ_Q by means of $H_{L\rho} = 1/\sqrt{3}\cdot(\Delta_D^2 + \Delta_Q^2)^{\frac{1}{2}}$ according to the general relation (equation 12).

For the measurement of the nuclear spin relaxation time in the rotating frame, $T_{1\rho}$, the spin-locking technique was used (see Fig. 5). A 90° pulse with an rf-field large compared to the internal field $H_{L\rho}$ along the x-direction rotates the nuclear magnetization from the direction of the static magnetic field to the y-direction. Immediately after the pulse, the rf-field is phase-shifted by 90° and reduced to a value of H_1. Now, H_1 lies parallel to the direction of the nuclear magnetization; the magnetization is called 'locked' in a frame rotating with the Lamor frequency ω_0. With respect to the rotating frame, H_1 plays the role of a time-independent field. Consequently, the rotating magnetization relaxes parallel to the locking field H_1 with a time constant $T_{1\rho}$, the relaxation time in the rotating frame. To measure $T_{1\rho}$, the nuclear magnetization is allowed to decrease in the presence of the locking field H_1 for some time t, then H_1 is turned off and the initial height (or the total area) of the nuclear free induction decay signal $F(t)$ is measured. According to Fig. 5 one has for $t = \tau_L$

$$F(\tau_L) = F(0)\exp(-\tau_L/T_{1\rho}). \tag{13}$$

An example of a typical $T_{1\rho}$-experiment at 77 K is depicted in Fig. 5. The figure shows the free induction decays of ^{27}Al in ultrapure aluminium after a spin-locking sequence without ($\dot\epsilon = 0$) and with ($\dot\epsilon = 3.6\,s^{-1}$) a finite plastic strain rate. The data were obtained in one single shot without repetition. It is obvious that an applied strain rate $\dot\epsilon$ causes a significant reduction in the relaxation time $T_{1\rho}$. As discussed above, from such experiments the dislocation-motion induced part of the relaxation rate, $(1/T_{1\rho})_D$ can be determined using equation (3).

According to equation (7), in the strong-collision region, a plot of the dislocation-induced contribution to $T_{1\rho}$ vs square of the locking field will yield a straight line which can be extrapolated to find the abscissa-intercept at $H_1^2 = -H_{L\rho}^2$. Figure 6 shows

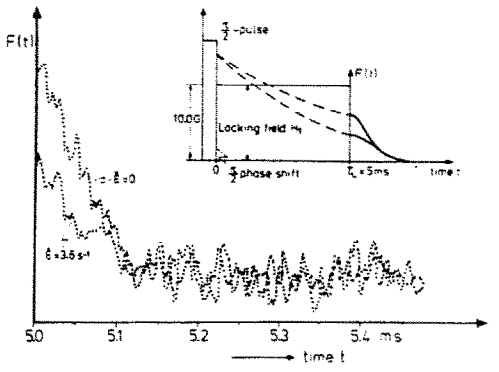

Fig. 5. Experimental result showing two free induction decays $F(t)$ after a spin locking sequence with zero and finite plastic deformation rate $\dot\epsilon$ in ^{27}Al (locking field $H_1 = 10\ G$; see insert).

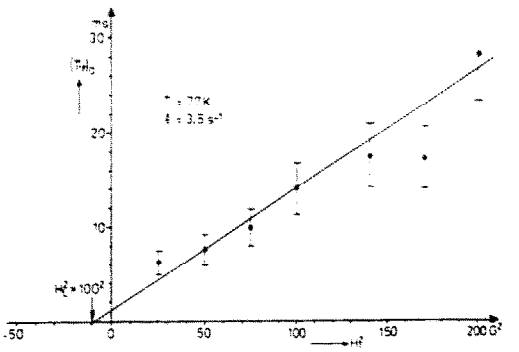

Fig. 6. Plot of the dislocation-induced contribution to the relaxation time $T_{1\rho}$ vs the locking field H_1^2 of ^{27}Al at a constant strain rate $\dot\epsilon$ at 77 K.

such a plot of $(T_{1\rho})_D$ of ultrapure aluminium at a constant strain rate $\dot\epsilon$ for $T = 77$ K. The local field $H_{L\rho}$ thus obtained is $H_{L\rho} = 3.16\ G$ in line with the data obtained from the line shape analysis of the spin echo signals (see Table 1) in the Al–Cu alloys.

In Fig. 7 the dislocation-induced contribution to the relaxation rate, $(1/T_{1\rho})_D$, measured with a constant locking field H_1 of 10 G is plotted as a function of plastic strain rate $\dot\epsilon$ for two different temperatures (77 K and 298 K). The slope of the curve up to $\dot\epsilon = 10\,s^{-1}$ is found to be proportional to the strain rate $\dot\epsilon$ as predicted by equation (7). As discussed in section 2, from the magnitude of the ratio $(1/T_{1\rho})_D/\dot\epsilon$ the mean jump distance L can be determined if the other parameters in equation (7) are known. Based on such experiments systematic measurements of the jump distance L in the different aluminium samples are presented and discussed in relation to transmission electron microscopic investigations in the next section.

In addition to the ^{27}Al measurements, analogously the first dynamic ^{51}V NMR measurements obtained from 3 N vanadium foils with a thickness of about 25 μ at $T = 298$ are included in Fig. 7. The data demonstrate the possibility for studying dislocation motion in other metallic systems by nuclear spin relaxation measurements. However, a quantitative

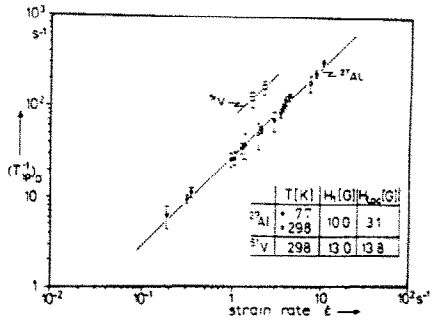

Fig. 7. Dislocation-induced part of the ^{27}Al and ^{51}V relaxation rates $(T_{1\rho}^{-1})_D$ in aluminium and vanadium as a function of $\dot\epsilon$ for different temperatures ($\epsilon \gtrsim 7\%$).

interpretation of the vanadium data has to take into account the b.c.c. structure of vanadium and the resulting different behaviour of moving dislocations compared to f.c.c. metals.

4. RESULTS AND DISCUSSION

4.2 *Mean jump distance of moving dislocations in Al*

As discussed above, from the magnitude of the slope of the curve $(T_{1\rho}^{-1})_D$ vs $\dot{\epsilon}$ the mean jump distance L can be obtained provided the other parameters in equation (7) are known. Taking the Schmid factor ϕ for polycrystalline f.c.c. material equal to 0.33 [23] and the data as given in section 3, the mean jump distance calculated from Fig. 7 is about 0.1 μm for $\epsilon \gtrsim 7\%$. The strain dependence of L has been obtained from measuring $T_{1\rho}^{-1}$ as function of strain ϵ. The results are depicted in Fig. 8.

The mean jump distance L measured by NMR in Al has to be interpreted with care in terms of mean slip distance and statistical slip length (Λ_{st}). As commonly found in annealed f.c.c. metals [24], a cell structure is formed in Al after deformation at room temperature and at 77 K. Cell structure formation involves easy cross slip of large numbers of screw dislocations, i.e. either cross slip of screw dislocations from pile-ups behind Cottrell–Lomer barriers (Seeger, [25]) or cross slip from the original slip planes to form relatively strain free cell walls

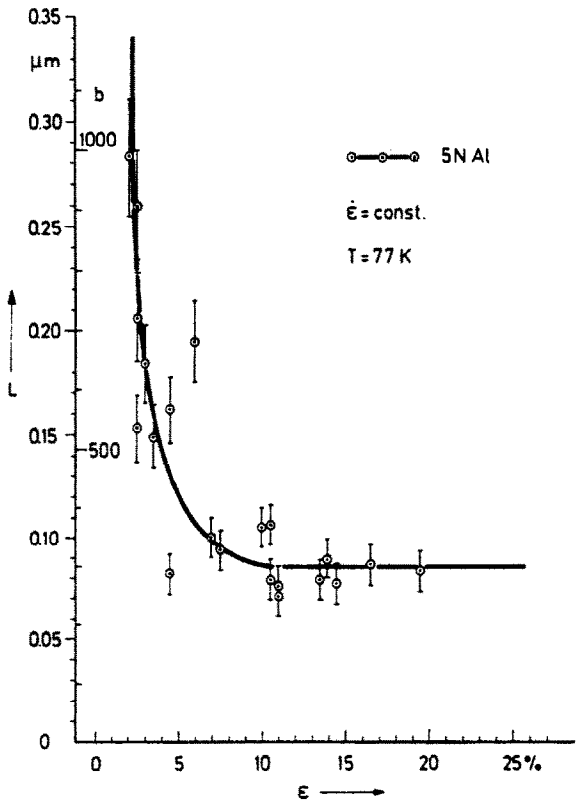

Fig. 8. The mean jump distance measured by NMR as a function of strain ϵ in Al.

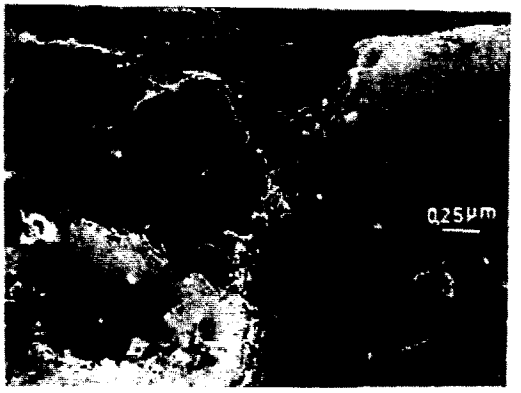

Fig. 9. Cell structure of Al deformed 15% at 77 K. Dark field/weak beam image, [100] orientation, g = [002], JEM 200 CX.

(Hirsch, [26]). Two electron micrographs illustrating the cell structure of deformed Al at 15% and at 25% strain are shown in Figs 9 and 10, respectively. The cells are relatively free from dislocations but are separated by walls of high dislocation density. The dislocation aggregation in the cell walls are tangles, jogged, twisted and mixed together in an irregular way. The cell diameter is for both degrees of deformation ranging from 1 to 2 μm. The speed of the mobile dislocation is reduced in the cell wall compared with that outside the cell wall. As a result, the mean slip distance of dislocations is mainly determined by the cell size when the cell structure is well developed. The statistical slip length Λ_{st} will be of the same order of magnitude as the cell size ($\simeq$1–2 μm) [27, 28], i.e. much larger than the mean jump distance measured by NMR ($\simeq$0.1 μm for $\epsilon \gtrsim 7\%$).

A plausible explanation for this difference is that all moving dislocations, present both in the cell boundary and in the interior region of the cell, affect the spin lattice relaxation rate. The mean jump distance of dislocations measured by NMR is possibly related to the spacing of the dislocation tangles near the cell boundary ranging from 0.01 to 0.1 μm. We assume the following model: a mobile dislocation crosses a cell

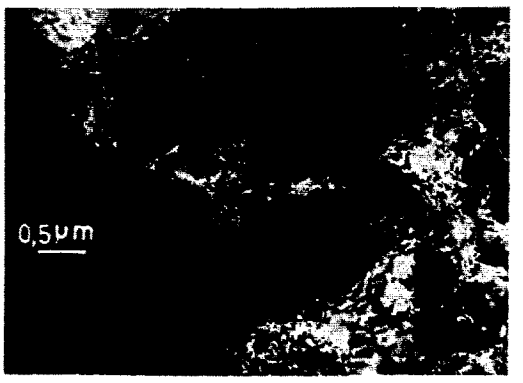

Fig. 10. Cell structure of Al deformed 25% at 77 K. Dark field/weak beam image, [100] orientation, g = [002]; JEM 200 CX.

by one step, i.e. the corresponding jump distance L_1 is of the order of the cell diameter ($\sim \Lambda_{st}$). Subsequently, many short jumps occur with a distance L_2 ($\simeq$ spacing of the tangles 0.01–0.1 μm). Assuming two different sets of corresponding mobile dislocation densities: ρ_1 in the interior of the cell and ρ_2 inside the cell wall the total spin lattice relaxation rate can be written as

$$\left(\frac{1}{T_{1\rho}}\right)_D = \left(\frac{1}{T_{1\rho}}\right)_D^{(1)} + \left(\frac{1}{T_{1\rho}}\right)_D^{(2)} \tag{14}$$

where

$$\left(\frac{1}{T_{1\rho}}\right)_D^{(1)} \sim \frac{g_Q(L_1)\rho_1}{L_1\rho} \quad \text{and} \quad \left(\frac{1}{T_{1\rho}}\right)_D^{(2)} \sim \frac{g_Q(L_2)\rho_2}{L_2\rho} \tag{15}$$

and $\rho = \rho_1 + \rho_2$. The dislocation density in the cell wall is about 5–6 times higher than in the interior region of the cell [24, 29–31]. Further, since $L_1 \gg L_2$ and $g_Q(L_1) \simeq 1$ and $g_Q(L_2) \simeq 0.6$ (Fig. 1) the total spin lattice relaxation rate measured by NMR is largely determined by the jump distance inside the cell wall

$$\left(\frac{1}{T_{1\rho}}\right)_D \simeq \left(\frac{1}{T_{1\rho}}\right)_D^{(2)}. \tag{16}$$

Another explanation for the difference between the jump distance L measured by NMR and the mean slip distance Λ_{st} can be based on a dislocation mechanism in which the dislocation free path Λ_{st} depends on the mobile dislocation density and the number of dislocation intersections, N_c. If the dislocations are delayed at each of these intersections during a period of time $\tau_c > 10^{-4}$ s, spin-lattice relaxation takes place in the strong collision approximation). As a result the spin-lattice relaxation rate $T_{1\rho}^{-1}$ is determined by the waiting time τ_c at each intersection. The dislocation mean jump distance L thus obtained is much smaller than the actual mean slip distance Λ_{st}. When N_c is about 10 the mean jump distance L measured by NMR would be one order of magnitude smaller than Λ_{st} as observed.

An argument that makes the former model somewhat favourable is that at small strains, i.e. before cells are being established, the mean jump distance is found to be much larger compared to L at large strains when distinct cells have been formed. In the former model one could expect that L decreases with increasing strains up to $\simeq 7\%$ which is indeed the case (Fig. 8). At strains larger than 7%, the dislocation cells shrink in size through the subdivision of the largest cells. Such subdivision ceases the cells have become so small that no new cell walls are being nucleated because chance encounters of glide dislocations have become negligibly small [32]. Therefore, the shrinking process of the cell pattern cannot go indefinitely and the cell diameter approaches an asymptotic value of 1–2 μm. It means that for strains larger than $\simeq 7\%$ the statistical slip distance Λ_{st} and the mean jump distance L measured by NMR are almost not strain dependent.

Further, during stage II hardening ($\epsilon < 7\%$) the storage of dislocations follows strictly geometrical or statistical rules which are not considerably influenced by temperature and strain rate. One of the characteristics of stage II hardening of pure f.c.c. metals is that the number of dislocations per slip line remains approximately constant and that the slip line lengths Λ_L decrease with increasing strain, both in theory [33] and experiment [34]. Assuming in stage II that the jump distance L is proportional to the statistical slip length Λ_{st} and that Λ_{st} is proportional to Λ_L it means that

$$\frac{1}{L} \sim \epsilon. \tag{17}$$

The flow stress can be expected to vary with dislocation density according to

$$(\tau - \tau_0) \sim \sqrt{\rho}. \tag{18}$$

In the beginning of deformation the statistical population of dislocations will be related to the statistical slip length and mean jump distance by

$$\sqrt{\rho} \sim \frac{1}{L} \tag{19}$$

leading to [35]

$$\tau = \tau_0 + k\epsilon. \tag{20}$$

From Fig. 8 we find indeed that the inverse of the mean jump distance varies linearly with strain according to equation (17). However, it should be noted that the behaviour of the statistical population at large strains is hardly likely to be well described in polycrystals as being similar to stage II hardening in single crystals [29, 36]. The mean free path of dislocations in polycrystals is not only defined by dislocation interaction [equation (19)] but also by additional barriers or sinks such as grain boundaries. Nevertheless, the NMR measurements confirm the findings obtained from slip line measurements [equation (17)] which suffer from the disadvantage that they are essentially surface observations of the slip-pattern at the surface. Furthermore, it has to be noted that pure Al was annealed at 290°C to avoid excessive grain growth. As a result, the 'yield stress' is high (Fig. 2). All of 'stage-II' hardening therefore could have happened during the annealed prestrain and consequently stage-II hardening cannot be associated with the first 7% of the observed strain.

So far we did not consider the detailed effect of grain sizes in polycrystalline Al. The mean free path obtained from the NMR measurements is far less (0.1 μm), compared to the grain size diameter $\simeq 150$ μm and thickness of the foils 50 μm.

However, even in the early stage of deformation, the grain boundaries limit dislocation movement

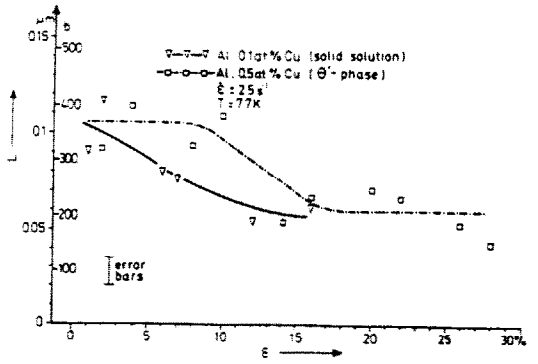

Fig. 11. The mean jump distance measured by NMR as a function of strain in Al:0.1 at.% Cu and Al:0.5 at.% Cu (θ').

resulting in an initial parabolic hardening instead of an easy glide region of single crystals. An aspect of complexity is that the stress system even within one grain is very heterogeneous and depends on the behaviour of the adjacent grains. In general these effects are likely to be more important at small grain sizes. So, we expect that the grain sizes taken will approach more closely the behaviour of single crystals [27, 37].

4.2 *Mean jump distance of moving dislocations in Al–Cu.* (0.1 *at.% Cu solution*)

In Fig. 11 the strain dependence of L in Al–0.1 at.% Cu (solid solution) as measured by NMR has been depicted. An electron micrograph illustrating Al–0.1 at.% Cu deformed at $T = 77$ K ($\epsilon = 16\%$) is shown in Fig. 12. The Al alloy containing Cu shows a distinct cell structure. In comparison with pure aluminium (see Fig. 9), there are, however, more dislocations inside the cells indicating a certain amount of dislocation pinning by the matrix. Further, the cell seems to have more ragged cell walls which are much wider than in pure aluminium. One of the reasons that cells are not readily formed in Al–Cu alloys could be the lowering of the stacking fault energy in Al ($\gamma_{SF} \simeq 200\,\mathrm{mJ/m^2}$) upon adding Cu ($\gamma_{SF} \simeq 40\,\mathrm{mJ/m^2}$) [38]. It is the stacking fault energy that determines whether or not a cell structure is formed. A lowering of the stacking fault energy impedes cross slip and the cell structure resulting from cross slipping screw dislocations is less readily formed. It should be noted, however, that the strength of aluminium alloys is largely determined by the atomic diameter of the solute element [39] in contrast to for example copper alloys [40]. Besides the lowering of the stacking fault energy making cross slip less favourable, the small strain fields around the solute atoms could prevent screw dislocations from becoming aligned along ⟨110⟩ directions for cross slip [25]. The stress at the beginning of the parabolic hardening (τ_{III}) is associated with onset of cross slip. Therefore, it follows that the addition of Cu to Al (Cu is about 10% smaller than Al) will raise the stress τ_{III} (see Fig. 2).

The binding energy between Cu and an edge dislocation in Al is rather small: 0.2 eV [41] at a distance $r \simeq \mathbf{b}$ (calculated using isotropic elasticity theory). Further, at 77 K the mobility of Cu impurities is too low to follow the mobile dislocations. The diffusion coefficient of Cu in *quenched* Al is $\simeq 10^{-16}\,\mathrm{cm^2/s}$ ($T_q = 550$°C) calculated from the activation energies for the migration and formation of vacancies (0.58 and 0.76 eV, respectively) [42] leading to a jump time for long range diffusion of Cu ions ($\simeq 16$ s) which is far more than the waiting time of mobile dislocations. Therefore, we may conclude that Cu will act as an immobile weak obstacle for mobile dislocations.

The mean jump distance measured by NMR ($\simeq 0.06\,\mu$m) is about one order of magnitude larger than the spacing between the Cu particles as calculated in the Friedel limit [43, 44] assuming that during the yielding process the dislocation takes up a steady-state configuration. The average spacing of the Cu particles in the slip plane is about 0.008 μm and the mean jump distance would be 0.005 μm. In conclusion we must say that the mean jump distance of dislocations in Al–0.1 at.% Cu is mainly determined by the dislocation density and dislocation distribution. The latter is directly affected by Cu, impeding the cross slip process and hampering the cell structure formation. The cell structure is more ragged than in pure Al, resulting in a smaller mean jump distance. The dislocation density for the same strain is increased locally leading to a smaller L value.

4.3 *Mean jump distance of moving dislocations in Al–1 at.% Cu*

The NMR results (L vs ϵ) obtained from Al–1 at.% Cu (solid solutions) are shown in Fig. 13.

An Al–1 at.% Cu alloy quenched from a solution treatment temperature of 550°C (2.5 h) has been examined in the electron microscope JEM 200CX after 14% elongation at 77 K. In contrast to Al and Al–0.1% Cu this alloy forms no cell structure at all (Fig. 14). The dislocations are uniformly distributed. The uniform distribution is interdispersed with loops. As in the previous discussion on Al–0.1% Cu, Cu sol-

Fig. 12. Al–0.1 at.% Cu (solid solution) deformed 16% at 77 K. Dark field/weak beam image, [100] orientation, g = [002]; JEM 200 CX.

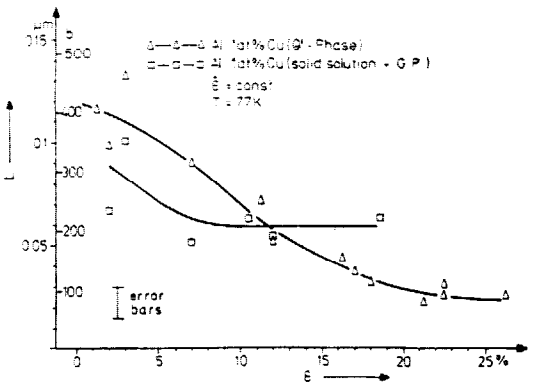

Fig. 13. The mean jump distance measured by NMR as a function of strain ϵ in Al: 1 at.% Cu (θ') and in Al: 1 at.% Cu (solid solution + G. P.).

ute atoms impede the cross slip process and as such hinder cell structure formation. In addition, quenching results in a supersaturation of point defects. Since Cu has a low solubility in Al at room temperature, the specimen had to be quenched to retain Cu in solid solution. Several workers [44–47] found that some of the point defects tend to condense into (vacancy) loops or onto screw dislocations to form helices. In Al–Cu alloys where the formation energy of vacancies is low and because of the solute-vacancy interactions a larger fraction of vacancies may be retained, the climb of the dislocations prevents the dislocations from cross slipping, i.e. hindering cell structure formation.

The diffraction pattern associated with Fig. 14. showed some streaking in the cubic directions indicating that coherent GP zones are being formed. A mobile dislocation cuts across the GP zone as across a forest dislocation of Burgers vector $\mathbf{b}_{GP}$. As Friedel discusses [43] two significant contributions to the elastic interaction must be added: modulus (μ) hardening and chemical hardening. Actually, a mobile dislocation is repelled by the zone in Al–Cu since $\mu_{Cu} > \mu_{Al}$. The chemical energy per solute atom gained when zones are formed is positive and the mobile dislocation is therefore hindered in its motion since energy must be spent to compensate for the loss in chemical energy. Fleischer [48] argues that the chemical strengthening is small because when the three orientations of the zones intersecting the slip planes are considered in detail, there is little net change in the number of copper-copper bonds when a dislocation sweeps over the slip plane (for a discussion see Kelly and Nicholson [42]). In addition, due to stacking fault hardening ($\gamma_{Al} > \gamma_{Cu}$) the dislocations may be attracted to the GP zones. All these factors which tend to hinder cell structure formation also increase the stress at which parabolic hardening occurs (see Fig. 2).

The mean jump distance measured by NMR is determined by the dislocation density, the distribution of dislocations and the size of the GP zones. The dislocation density for the same strain is increased compared to pure Al. Assuming a parabolic relation $\tau \sim \sqrt{\rho}$, from Fig. 2 one obtains: $\rho_{Al} \simeq 0.4\ \rho_{Al-1\ at.\%\ Cu}$. Assuming a statistical distribution of dislocations

$$L \sim \rho^{-\frac{1}{2}}$$

it follows

$$\left(\frac{L_{Al}}{L_{Al-1\ at.\%Cu}}\right) = 1.6$$

calculated using the data shown in Fig. 2. The NMR experiments yield (see Fig. 13)

$$\left(\frac{L_{Al}}{L_{Al-1\ at.\%Cu_{NMR}}}\right) = 1.7.$$

The agreement is excellent.

4.4 *Mean jump distance of moving dislocations in Al–1 at.% Cu containing θ′ precipitates*

In Fig. 13 the NMR results are displayed in the case of Al–1 at.% Cu (θ' phase). Figure 15 shows an

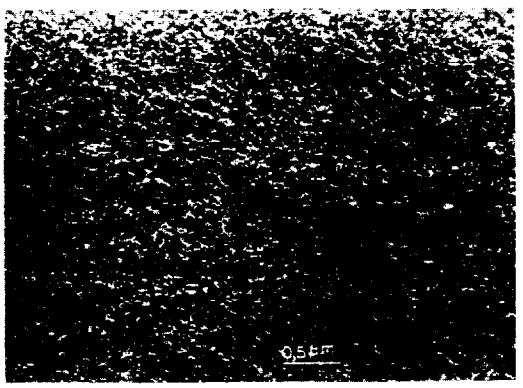

Fig. 14. Al–1 at.% Cu (solid solution + G. P.) deformed 14% at 77 K, dark field weak beam, [100] orientation, g = [002], JEM 200 CX.

Fig. 15. Al–1 at.% Cu (θ' phase), 26% deformation. Bright field/strong beam image, [100] orientation, g = [002]; JEM 200 CX.

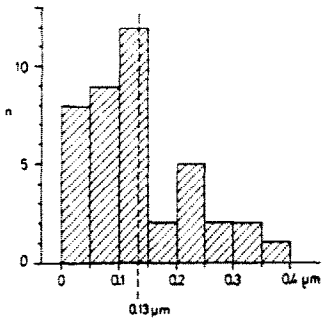

Fig. 16. Histogram of the distribution of interspacing distances between the θ' plates in Al–1 at.% Cu as shown in Fig. 15.

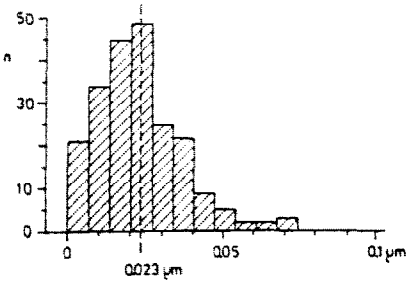

Fig. 18. Histogram of the interspacings between the dislocation loops in Al:1 at.% Cu, lying in the area indicated in Fig. 17.

electron micrograph of Al–1 at.% Cu. The typical microstructure shows plate-like θ' precipitates which are partially coherent: coherent on one {100} and semicoherent (interfacial dislocations) on the remaining two cubic planes {100}. It is well known [42, 49] that the strong plates of the θ' phase show the effect expected of a plastically nonhomogeneous material. Al–Cu alloys containing thick θ' plates deform by the Orowan process [50]. The stress-strain curve of Al–Cu θ' phase is similar in shape to that of an alloy containing the non-coherent θ phase. According to Russell and Ashby [49] the interplate spacing in the slip direction (Λ_g) sets an upper limit for the slipdistance, i.e. the actual distance traversed before it gets stuck. The mean distance between the plates is about 0.13 μm (see Fig. 16). So, we expect that the mean jump distance at the beginning of deformation is determined by this upper limit $\simeq$0.13 μm. By NMR measurement a value of 0.12 μm has been obtained for the mean jump distance. The hardening is thus controlled by the microstructure at the beginning of deformation.

The dislocation configuration after an elongation of 20% at 77 K in the same material has been depicted in Fig. 17. A distribution of dislocations is found which is to some extent rather uniform and which is interdispersed with loops. Ashby [49, 51] made the important distinction between 'statistically stored' dislocations, i.e. those that would accumulate during simple tension and 'geometrically necessary' dislocations, i.e. those generated in addition to the statistical dislocations to accomplish the rotation of the nondeforming plates during deformation. The density of the geometrically necessary dislocation can be very high: plates spaced 0.13 μm apart require a density of about 10^{12} cm^{-2} to accomodate the lattice curvature resulting from 20% strain. This is much larger than the density of 10^{10} cm^{-2} of dislocations which are statistically stored in an Al crystal at similar strains. Because arrays of geometrically necessary dislocations are formed during straining, dislocations are stored more rapidly with strain in Al–1 at.% Cu containing θ' plates than in identical solid solutions. As a result the shear stress τ of the aged alloy containing θ' precipitates is higher than of Al–1 at.% Cu solid solution (Fig. 2).

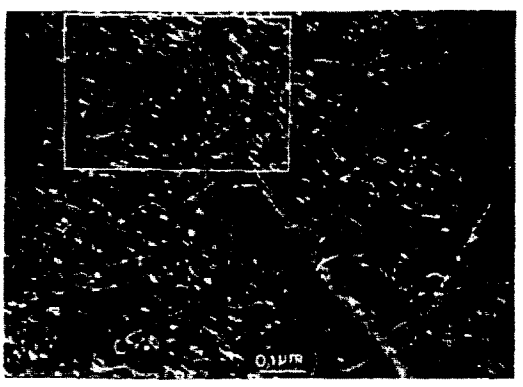

Fig. 17. Al–1 at.% Cu (θ' phase), 20% deformation at 77 K. Dark field/weak beam image, [100] orientation, g = [002]; JEM 200 CX.

The shear-stress shear-strain equation obtained using Ashby's concept is given by

$$\tau = \tau_0 + \alpha\mu b\left(\frac{a}{4b\Lambda_g} + \frac{a}{b\Lambda_{st}}\right)^{\frac{1}{2}}. \qquad (21)$$

It should be noted at this point that Λ_g, defined by Ashby as a constant, is independent of the shear strain a. Thompson *et al.* [27] proposed a modification to the Ashby view point where Λ_g sets an upper limit to Λ_{st} and $\Lambda_{st} \simeq \Lambda_g$ at yield. Then at small strain the slip distance is $\simeq\Lambda_g$ and at large strain where $\Lambda_{st} \ll \Lambda_g$ it reduces to $\tau \sim \Lambda_{st}^{-1}$. This situation has been found in our experiments. At the beginning of deformation $L_{NMR} \simeq \Lambda_g$. At larger strains the mean distance between the statistical dislocations is about 0.023 μm (see Figs 17 and 18) whereas $L_{NMR} \simeq 0.03$ μm (Fig. 13).

4.5 *Mean jump distance of moving dislocations in Al–0.5 at.% Cu*

In Fig. 11 the mean jump distance in Al–0.5 at.% Cu measured by NMR as a function of strain has been depicted. A transmission electron micrograph of Al–0.5 at.% Cu deformed 25% at 77 K is shown in Fig. 19. θ' plates have been detected (using strong

Fig. 19. Al—0.5 at.% Cu (θ' phase), 25% deformation at 77 K. Dark field/weak beam image, [110] orientation, $g = [1\bar{1}1]$; Philips EM 300.

beam) with an interplate space of 1–5 μm. From Fig. 19 it is clear that cell formation is still present as in pure Al and Al–0.1 at.% Cu solid solution. The cell diameter is of the same order of magnitude as in pure Al. However, the cell walls are much thicker than in pure Al and there are more dislocations inside the cells indicating a certain amount of dislocation pinning by the matrix. Since $\Lambda_{st} \lesssim \Lambda_g$ the hardening is controlled by the matrix itself. Therefore, the mean jump distance at the beginning of deformation approximates the mean jump distance in Al–0.1 at.% Cu. At higher strains more ragged cells are formed due to the presence of Cu in solid solution leading to a decrease of the mean jump distance as measured by NMR (see Fig. 11).

5. CONCLUSIONS

The conclusion may be drawn that pulsed nuclear magnetic resonance is a complementary new technique for the study of dislocations in metallic systems. Since the process of dislocation motion is made up of atomic movements nuclear magnetic resonance technique offers a possibility to determine the manner in which dislocations progress through the crystal as a function of time utilising nuclear spin relaxation as a tool.

It turned out that from the pulsed nuclear magnetic resonance experiments on Al and Al–Cu alloys the following mean jump distance of moving dislocations can be deduced:

(a) Al: ranging from 0.28 μm at small strains to 0.09 μm at large strains (Fig. 8).
(b) Al–0.1 at.% Cu (solid solution), ranging from 0.11 μm at small strains to 0.06 μm at large strains (Fig. 11).
(c) Al–1 at.% Cu (solid solution + GP zones) in the range of 0.09 μm at small strains to 0.06 μm at large strains (Fig. 13).
(d) Al–1 at.% Cu (θ' phase): varying from 0.12 μm at small strains to 0.03 μm at large strains (Fig. 13).
(e) Al–0.5 at.% Cu (solid solution + θ' phase): ranging from 0.11 μm at 2% strain to 0.06 μm at strains larger than 15% (Fig. 11).

Acknowledgements—The authors wish to thank Dr H. J. Hackelöer for his technical assistance in the NMR measurements and Mr G. J. L. Van Der Wegen for preparing the electronmicrographs. Particular thanks are due to Mr H. J. Bron, Mr U. B. Nieborg and Mr J. Harkema for their technical assistance in preparing and analyzing the specimens. This work is part of the research program of the Foundation for Fundamental Research on Matter (F.O.M.—Utrecht) and has been made possible by financial support from the Netherlands Organization for the Advancement of Pure Research (Z.W.O.—The Hague) and the Deutsche Forschungsgemeinschaft, F.R.G.

REFERENCES

1. E. Orowan, *Z. Phys.* **89**, 634 (1934).
2. W. G. Johnston and J. J. Gilman, *J. appl. Phys.* **30**, 129 (1959).
3. R. R. Neuhäuser, *Physica status solidi a* **24**, 549 (1974).
4. D. R. James and S. H. Carpenter, *J. appl. Phys.* **42**, 4685 (1971).
5. T. Imanaka, K. Sano and M. Shimizu, *Cryst. Latt. Defects* **4**, 57 (1973).
6. A. Granato and K. Lücke, *J. appl. Phys.* **27**, 583 (1956).
7. N. K. Chen and R. Maddin, *Prog. Metal Phys.* **5**, 53 (1956).
8. P. Hirsch, A. Howie, R. B. Nicholson, D. W. Pashley and M. J. Whelan, in *Electron Microscopy of Thin Crystals*, Kreiger, New York (1977).
9. G. Hut, Thesis, University of Groningen (1976).
10. W. H. M. Alsem, J. Th. M. De Hosson, H. Tamler, H. J. Hackelöer and O. Kanert, in *Nuclear and Electron Resonance Spectroscopies Applied to Materials Science* (edited by E. N. Kaufmann and G. K. Shenoy), p. 481. North Holland, Amsterdam (1981).
11. H. Tamler, H. J. Hackelöer, O. Kanert, W. H. M. Alsem and J. Th. M. De Hosson, in *Nuclear and Electron Resonance Spectroscopies Applied to Materials Science* (edited by E. N. Kaufmann and G. K. Shenoy), p. 421. North Holland, Amsterdam (1981).
12. J. Th. M. De Hosson and O. Kanert, in *Dislocations in Solids* (edited by F.R.N. Nabarro). To be published.
13. D. Wolf, in *Spin Temperature and Nuclear Spin Relaxation in Matter*. Clarendon Press, Oxford (1979).
14. D. Wolf and O. Kanert, *Phys. Rev.* **B16**, 4776 (1977).
15. O. Kanert and M. Mehring, *Static Quadrupole Effects in Disordered Cubic Solids, NMR Vol. 3, p. 40*. Springer Verlag, Berlin (1971).
16. O. Kanert and K. Preusser, *Solid St. Commun.* **15**, 97 (1974).
17. R. H. Beton and E. C. Rollason, *J. Inst. Metals* **86**, 77 (1957–58).
18. E. Hornbogen, *Aluminium* **43**, 9 (1976).
19. J. H. Van Vleck, *Phys. Rev.* **74**, 1168 (1948).
20. T. J. Rowland and F. Y. Fradin, *Phys. Rev.* **182**, 760 (1969).
21. T. S. Lundy and J. F. Murdock *J. appl. Phys.* **33**, 1671 (1962).
22. N. L. Peterson and S. J. Rothman, *Phys. Rev.* **B2**, 3264 (1970).
23. P. Haasen, in *Physikalische Metallkunde*, p. 280. Springer-Verlag, Berlin (1974).
24 P. R. Swann, in *Electron Microscopy and Strength of Crystals* (edited by G. Thomas and J. Washburn), p. 131. Wiley, New York (1963).

25. A. Seeger in *Dislocations and Mechanical Properties of Solids* (edited by J. C. Fischer, W. G. Johnston, R. Thompson and T. Vreeland) Wiley, New York (1956) 243.
26. P. B. Hirsch, in *The Physics of Metals* (edited by P. B. Hirsch), Vol. 2, p. 189. Cambridge Univ. Press (1975).
27. A. W. Thompson, M. I. Baskes and W. F. Flanagan, *Acta metall.* **25,** 1017 (1973).
28. H. Fujita and T. Tabata, *Acta metall.* **21,** 355 (1973).
29. A. S. Keh and S. Weissmann, in *Electron Microscopy and Strength of Crystals* (edited by G. Thomas and J. Washburn), p. 231. Wiley, New York (1963).
30. J. E. Bailey, *Phil. Mag.* **8,** 223 (1963).
31. F. H. Hammad and W. D. Nix, *Trans. Am. Soc. Metals* **10,** 94 (1966).
32. D. Kuhlman-Wilsdorf, in *Workhardening in Tension and Fatigue* (edited by A. W. Thompson), p. 1. Am. Inst. Min. Engrs (1977).
33. P. B. Hirsch and T. E. Mitchell, in *Workhardening*, p. 65. Gordon & Breach, London (1968).
34. S. Mader, in *Electron Microscopy and the Strength of Crystals* (edited by G. Thomas and J. Washburn), p. 183. Interscience, New York (1963).
35. B. Jaoul, *J. Mech. Phys. Solids* **5,** 95 (1957).
36. R. L. Jones and H. Conrad, *Trans. Am. Inst. Min. Engrs* **245,** 779 (1969).
37. N. Hansen, *Acta metall.* **25,** 863 (1977).
38. P. C. J. Gallagher, *Metall. Trans.* **1,** 2429 (1970) and references therein.
39. J. E. Dorn, P. Pietrokowsky and T. E. Tietz, *J. Metals* **188,** 933 (1950).
40. N. P. Allen, T. H. Scholfield and A. E. L. Tate, *Nature* **168,** 378 (1951).
41. J. P. Hirth and J. Lothe, in *Theory of Dislocations*, p. 462. McGraw–Hill, New York (1968).
42. A. Kelley and R. B. Nicholson, in *Progress in Materials Science* (edited by B. Chalmers), Vol. 10, p. 173. Pergamon Press, Oxford (1966).
43. J. Friedel, in *Dislocations*, Chaps 13 and 14. Pergamon Press, Oxford (1967).
44. F. R. N. Nabarro, *Phil. Mag.* **35,** 613 (1977).
45. G. Thomas and M. J. Whelan, *Phil Mag.* **4,** 511 (1959).
46. G. Thomas, *Phil. Mag.* **4,** 1213 (1959).
47. R. E. Smallman, K. H. Westmacott and J. A. Coiley, *J. Inst. Metals* **88,** 127 (1960).
48. R. L. Fleischer, in *Electron Microscopy and the Strength of Crystals* (edited by G. Thomas and J. Washburn), p. 973. Interscience, New York (1963).
49. K. C. Russell and M. F. Ashby, *Acta metall.* **18,** 891 (1970).
50. L. M. Brown and R. K. Ham in *Strengthening Methods in Crystals* (edited by A. Kelley and R. B. Nicholson), p. 37. Applied Science, London (1971).
51. M. F. Ashby, *Phil. Mag.* **21,** 399 (1970).